Check for updates

ChemPhotoChem

Research Article
doi.org/10.1002/cptc.202400113

Chemistry Europe
European Chemical Societies Publishing

www.chemphotochem.org

Room-Temperature Afterglow Nanostructures via Block Copolymer Self-Assembly

Yue Zhang[+],[a] Xiuzheng Chen[+],[a] Tengyue Wang,[a] Zhe Mo,[a] Guangming Wang,[a] Haodong Li,*[a] and Kaka Zhang*[a]

Miniaturization of organic afterglow materials has shown promising application in biomedical and other areas. Current technologies, such as nanoprecipitation, mechanical treatment, and emulsion polymerization, lack the capability of facile control on the morphology and dimension of the miniaturized organic afterglow materials. Here we report the fabrication of organic afterglow nanostructures via block copolymer self-assembly at room temperature. The fabrication is based on two-component design strategy where hydrophobic luminescent emitters with small rate constants of phosphorescence decay or reverse intersystem crossing are designed as the first component. Amphiphilic block copolymers that can form spherical core-shell micelles and worm-like micelles with glassy hydrophobic cores are used as the second component. Upon addition of water into a dimethylformamide solution that contains the two components, the amphiphilic block copolymers self-assemble into well-defined nanostructures and accommodate the hydrophobic luminescent emitters in nanostructure's hydrophobic cores. After switching to pure water by dialysis, room-temperature afterglow nanostructures have been obtained because of the excellent protection of organic triplets by the glassy hydrophobic cores. The afterglow nanostructures exhibit intriguing afterglow mechanism modulated by the types of luminescent emitters, controlled dimensions and morphologies by the structural parameters of the block copolymers.

Introduction

Room-temperature phosphorescence (RTP) materials, as well as organic afterglow materials, have aroused tremendous interest from both fundamental and application aspects.[1–14] Such materials feature long-lived excited states, sometimes with emission lifetimes of hundred milliseconds and even several seconds, which is distinct from fluorescence materials. Pioneering studies show that the incorporation of heavy atom effects (using bromo and iodine substitution and others) and n-π* transition (using aldehyde and ketone functional groups and others) can enhance intersystem crossing (ISC) and phosphorescence decay.[15–24] When nonradiative decay is suppressed by rigid environment (in crystals and glassy matrices), room-temperature phosphorescence and organic afterglow materials can be produced.[25–30] Various design strategies based on aggregation control,[31] supramolecular chemistry,[32–34] intermolecular charge transfer,[35–40] matrix's T_1 mediation,[41] dipole-dipole interaction,[42–45] sensitization and energy transfer[46–50] have been developed to fabricate organic RTP and afterglow materials with diverse structures and functions.[51–57]

Recently, miniaturization of organic RTP and afterglow materials has emerged as an interesting and important topic because of its application potential in biomedical and other fields.[49,51,58,59] Ultrafine particles have been reported to exhibit unique pathways for entering biological systems (such as enhanced permeation and retention effect) and for exclusion from living systems.[60–63] Nanosized materials that possess large specific surface areas have been found to show fast response to environment changes.[58,59] Nanomaterials with specific morphology may exhibit intriguing rheology behavior and biodistribution property.[64,65]

Nanoprecipitation method, that is, adding solution of RTP emitters into aqueous medium, allows the preparation of nanoscale and microscale RTP materials with emission lifetimes mostly in the millisecond region.[21,29,66] Mechanical grinding and ultrasonication in the presence of surfactants have been reported to disrupt RTP materials into small pieces in aqueous medium.[9,42,49] Usually, microparticles with irregular shapes or nanospheres can be obtained by the mechanical treatments. The fabrication of aqueous afterglow materials via emulsion polymerization developed by us shows that spherical afterglow latexes with sizes of around 100 nm can be readily obtained with emission lifetimes up to several seconds.[59,67,68] However, when compared to the well-established methods in nanoscience and nanotechnology, the miniaturization of organic RTP and afterglow materials is still in a very preliminary stage, where nanosized afterglow materials with diverse compositions, controlled sizes and well-defined morphologies are much less explored.

Block copolymer self-assembly has been widely applied to fabricate nanostructures with controlled dimensions and diverse morphologies.[69–74] Besides single-component system,

[a] Y. Zhang,[+] X. Chen,[+] T. Wang, Z. Mo, G. Wang, H. Li, K. Zhang
State Key Laboratory of Organometallic Chemistry, Key Laboratory of Synthetic and Self-Assembly Chemistry for Organic Functional Molecules, Shanghai Institute of Organic Chemistry, University of Chinese Academy of Sciences, Chinese Academy of Sciences, 345 Lingling Road, Shanghai 200032, People's Republic of China
E-mail: lihaodong@sioc.ac.cn
zhangkaka@sioc.ac.cn

[+] equal contribution.

Supporting information for this article is available on the WWW under https://doi.org/10.1002/cptc.202400113

© 2024 Wiley-VCH GmbH

23670932, 0, Downloaded from https://chemistry-europe.onlinelibrary.wiley.com/doi/10.1002/cptc.202400113 by Shanghai Institute Of Organic Chemistry, Wiley Online Library on [30/08/2024]. See the Terms and Conditions (https://onlinelibrary.wiley.com/terms-and-conditions) on Wiley Online Library for rules of use; OA articles are governed by the applicable Creative Commons License

two-component systems connected by non-covalent interactions have also been shown to exhibit strong capability to construct well-defined and functional nanostructures.[75,76] It has been reported by us and others that luminescent nanostructures can be achieved by modulating the non-covalent interactions in the two-component system of block copolymers and luminescent small molecules,[77–81] whereas room-temperature afterglow nanostructures (with emission lifetimes longer than 0.1 s) have not been realized in block copolymer self-assembly systems. It should be noted that there are some reported organic systems where block copolymers such as Pluronic F-127 are only used as surfactant to disperse afterglow nano-/micro-particles;[49] strictly speaking, such surfactant systems don't belong to block copolymer self-assembly system.

Here we report the fabrication of room-temperature afterglow nanostructures via block copolymer self-assembly in aqueous medium. Amphiphilic block copolymers and hydrophobic afterglow emitters are first dissolved in a common solvent (here dimethylformamide, DMF) and then added to selective solvent (here deionized water). Upon self-assembly, the hydrophobic blocks organize into well-defined hydrophobic domains that can also accommodate the hydrophobic afterglow emitters and protect the afterglow emitter from nonradiative decay (Figure 1). The size of the resultant afterglow nanostructures can be controlled by the length of the block copolymers and the morphology (spherical and worm-like) can be modulated by the structural parameters of the block copolymers. Interestingly, the afterglow mechanism, either room-temperature phosphorescence or thermally activated delayed fluorescence (TADF) afterglow, can be designed by using specific afterglow emitters.

Results and Discussion

Molecular Design and Synthesis

Poly(ethylene glycol)-*block*-poly(methyl methacrylate) (PEG-*b*-PMMA) amphiphilic block copolymers are selected in the present study. PMMA is hydrophobic and has glassy transition temperature of 110 °C. In aqueous medium, the hydrophobic PMMA blocks can form glassy domains to host hydrophobic afterglow emitters to protect organic triplet excited states by rigid microenvironment. PEG is a frequently used water-soluble polymer, which is nonionic and provides excellent solubility for self-assembly system. A series of PEG-*b*-PMMA block copolymers with different structural parameters are synthesized via PEG end group modification and then reversible addition-fragmentation chain transfer (RAFT) polymerization as shown in Figure 2. The detailed synthesis and purification procedures can be found in experimental section.

For the afterglow emitter, spiroBF$_2$ was first selected (Figure 2b). The spiroBF$_2$ molecules that are developed by our group show intramolecular charge transfer character from aromatic functional group to the electron-deficient dioxaborine group. There are ISC channels from S_1 state to T_n states with reasonable spin-orbital coupling matrix elements (SOCME) which allow the population of T_1 states (Figure S6).[42] Upon doping into suitable matrices where nonradiative decay of organic triplets can be effectively suppressed, the spiroBF$_2$ molecules would exhibit significant organic afterglow with mainly RTP emission in delayed spectra. The spiroBF$_2$ molecules can be readily synthesized by our cascade reaction in one pot manner.[42] It should be noted that spiroBF$_2$ molecules in solution state and solid state at room temperature don't show afterglow.

Self-Assembly of Block Copolymers and Afterglow Emitters

PEG-*b*-PMMA and spiroBF$_2$ were dissolved in DMF to give a mixed solution of concentrations 5 mg/mL and 0.1 or 0.15 mg/mL, respectively. To initiate the self-assembly, deionized water was added dropwise into the DMF solution under magnetic stirring. At water content of around 10 vol%, the sample already became turbid or bluish, which suggest the formation of micro- or nano-objects in the system. After reaching 50 vol% water content, the sample was stirred for additional 2 h and then transferred to a dialysis tube. DMF in the system can be completely removed by dialysis against deionized water for 3 days; deionized water for dialysis was updated every 8 h. PEG$_{44}$-*b*-PMMA$_{35}$, PEG$_{44}$-*b*-PMMA$_{52}$, PEG$_{44}$-*b*-PMMA$_{136}$, and PEG$_{44}$-

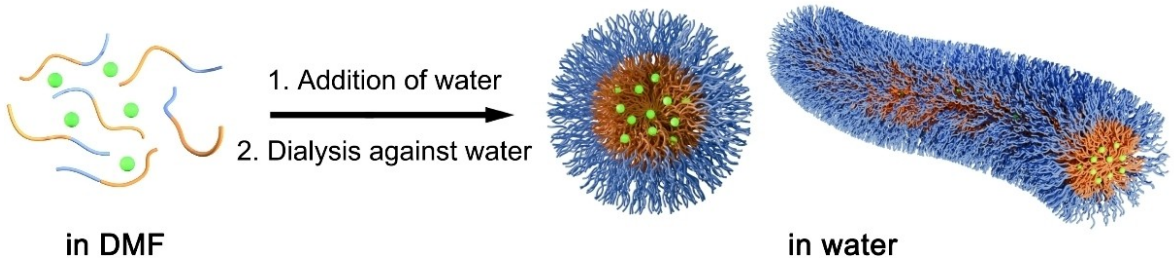

Figure 1. Fabrication of room-temperature afterglow nanostructures via block copolymer self-assembly. The hydrophobic afterglow emitters (green dots) dissolved in DMF don't show room-temperature afterglow because of active nonradiative decay in solution state. Upon water addition, the hydrophobic afterglow emitters can be encapsulated in the formed block copolymer nanostructures (blue chain, hydrophilic block; orange chain, hydrophobic block), locating in the core region of the nanostructures. After dialysis against water, the core region of the nanostructures becomes very rigid to suppress nonradiative decay of the hydrophobic afterglow emitters, leading to room-temperature afterglow in aqueous medium. The morphology of afterglow nanostructure, spherical core-shell and worm-like micelles, can be controlled by structural parameters of the amphiphilic block copolymers.

© 2024 Wiley-VCH GmbH

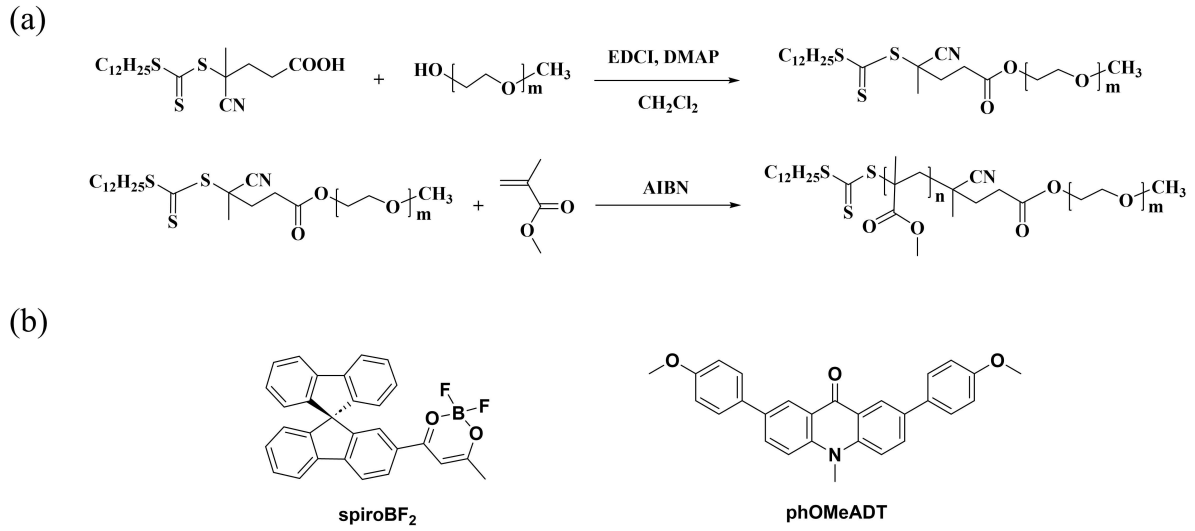

Figure 2. (a) Synthetic route of PEG-*b*-PMMA amphiphilic block copolymers. EDCI and DMAP represent 1-ethyl-3-(3-dimethylaminopropyl) carbodiimide hydrochloride and 4-dimethylaminopyridine, respectively. (b) Molecular structures of afterglow emitters in the present study.

b-$PMMA_{203}$ (the subscripts represent average degree of polymerization of each block) were used to assemble with spiroBF_2. The resultant spiroBF_2-PEG_{44}-*b*-$PMMA_{35}$ and spiroBF_2-PEG_{44}-*b*-$PMMA_{52}$ samples didn't show room-temperature afterglow even in degassed condition. The $PMMA_{35}$ and $PMMA_{52}$ blocks may be not long enough to form a rigid environment to protect spiroBF_2's triplets. PMMA is a plastic at room temperature. In the present study, rigid environment refers to the glassy environment of PMMA. The glass transition temperature of PMMA increases with molecular weight and levels off at high molecular weight.[43] For relatively short PMMA chains, the glass transition temperature is sensitive to molecular weight. Here the $PMMA_{35}$ and $PMMA_{52}$ blocks may be not long enough to form a rigid environment to protect spiroBF_2's triplets, when compared to $PMMA_{86}$, $PMMA_{136}$, and $PMMA_{203}$. The spiroBF_2-PEG_{44}-*b*-$PMMA_{136}$ and spiroBF_2-PEG_{44}-*b*-$PMMA_{203}$ samples exhibit afterglow at room temperature. Their steady-state emission spectra show spiroBF_2's fluorescence in the range of 400 nm to 550 nm with emission maxima at about 450 nm, while the delayed emission spectra (1 ms delay) exhibit spiroBF_2's phosphorescence ranging from 500 nm to 650 nm in degassed condition (Figure 3a and 3c). The phosphorescence band features emission maxima at approximately 540 nm and emission shoulders at 572 nm, which is typical for spiroBF_2's T_1 to S_0 radiative decay (Figure 3e) and agrees well with our previous studies on spiroBF_2-matrix RTP systems.[42] The average RTP lifetimes can be estimated from the emission decay profiles to be 546 ms and 873 ms for spiroBF_2-PEG_{44}-*b*-$PMMA_{136}$ and spiroBF_2-PEG_{44}-*b*-$PMMA_{203}$ samples, respectively (Figure 3b and 3d). Despite of the presence of organic afterglow property, these two samples are turbid and would form precipitates after long-term standing (Figure 4a, 4b and 4d), which suggest the formation of objects of tens of micrometers in the system. This should be caused by the large ratio of hydrophobic PMMA blocks over hydrophilic PEG blocks; the short PEG chains are not able to sufficiently stabilize the long PMMA blocks in aqueous medium.

By increasing PEG length, the resultant spiroBF_2-PEG_{113}-*b*-$PMMA_{86}$ sample in pure water has been found to be bluish and long-term stability (without precipitation, Figure 4c and 4d) and significant room-temperature afterglow in degassed condition (Figure 4e). Its steady-state and delayed emission spectra are similar to those of spiroBF_2-PEG_{44}-*b*-$PMMA_{136}$ and spiroBF_2-PEG_{44}-*b*-$PMMA_{203}$ samples (Figure 4f). Interestingly, its average RTP lifetime reaches 1121 ms as estimated from the excited state decay profile (Figure 4g). The balanced lengths of PEG and PMMA blocks may allow the compact packing of PMMA blocks to better protect spiroBF_2's triplets. To verify the colloidal stability, we prepare fresh spiroBF_2-PEG_{113}-*b*-$PMMA_{86}$ sample. To speed the dialysis process, we change water in the container every hour in the first three hours, then allow the dialysis overnight, and finally change water every four hours; in this way, the dialysis can be done in 24 hours. DLS measurement of the spiroBF_2-PEG_{113}-*b*-$PMMA_{86}$ sample has been performed to give a hydrodynamic diameter of 121.3 nm (polydispersity index of 0.227, Figure S7a). After storage for 24 hours, DLS shows a hydrodynamic diameter of 122.9 nm (polydispersity index of 0.218, Figure S7b), which indicates the colloidal stability of the spiroBF_2-PEG_{113}-*b*-$PMMA_{86}$ sample. TEM observation of spiroBF_2-PEG_{113}-*b*-$PMMA_{86}$ sample shows spherical morphology with an average diameter of 126 nm (Figure S8), which is consistent with DLS studies. It is noteworthy that the morphology and diameter of spiroBF_2-PEG_{113}-*b*-$PMMA_{86}$ sample are different from those of phOMeADT-PEG_{113}-*b*-$PMMA_{86}$ sample (*vide infra*), although the same polymer is used. The fast dialysis rate in spiroBF_2-PEG_{113}-*b*-$PMMA_{86}$ system leads to kinetic product that usually exhibit spherical morphology, while the slow dialysis in phOMeADT-PEG_{113}-*b*-$PMMA_{86}$ system produces worm-like morphology that is thermodynamic product (*vide infra*).

© 2024 Wiley-VCH GmbH

23670932, 0, Downloaded from https://chemistry-europe.onlinelibrary.wiley.com/doi/10.1002/cptc.202400113 by Shanghai Institute Of Organic Chemistry, Wiley Online Library on [30/08/2024]. See the Terms and Conditions (https://onlinelibrary.wiley.com/terms-and-conditions) on Wiley Online Library for rules of use; OA articles are governed by the applicable Creative Commons License

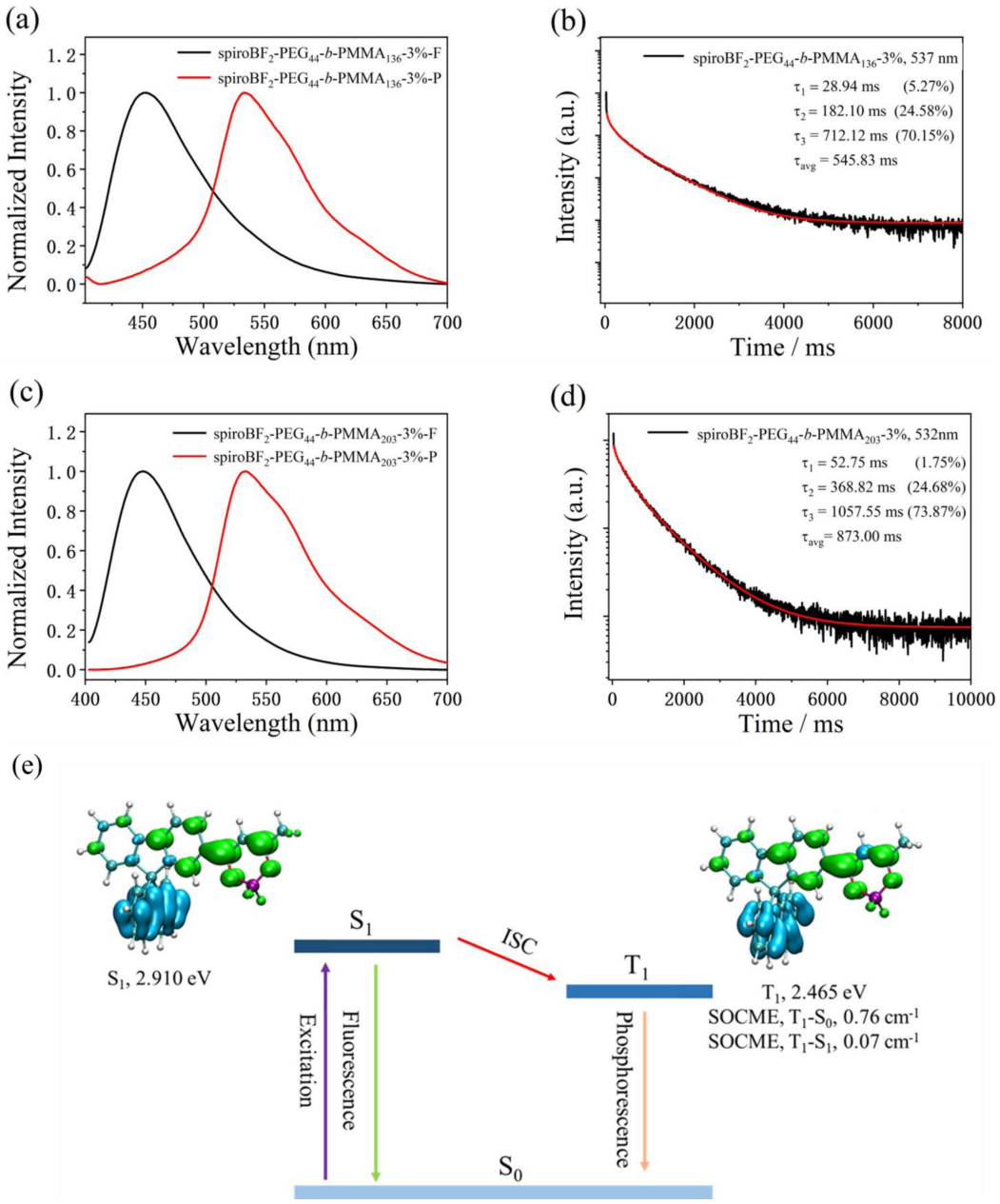

Figure 3. (a) Steady-state emission and delayed emission (1 ms delay) spectra of spiroBF$_2$-PEG$_{44}$-*b*-PMMA$_{136}$-3% sample excited by 383 nm at room temperature. (b) Excited state decay profile of spiroBF$_2$-PEG$_{44}$-*b*-PMMA$_{136}$-3% sample excited by 383 nm and monitored at 537 nm at room temperature. (c) Steady-state emission and delayed emission (1 ms delay) spectra of spiroBF$_2$-PEG$_{44}$-*b*-PMMA$_{203}$-3% sample excited by 372 nm at room temperature. (d) Excited state decay profile of spiroBF$_2$-PEG$_{44}$-*b*-PMMA$_{203}$-3% sample excited by 372 nm and monitored at 532 nm at room temperature. (e) The proposed mechanism of the room temperature phosphorescence.

TADF Afterglow Nanostructures

For organic RTP afterglow emitters in rigid environment, the phosphorescence lifetimes can reach 1.0 s and even longer because of the slow phosphorescence decay in organic systems. RTP afterglow emitters usually possess large Stokes shift that can minimize the influence of excitation lights. However, in some cases, the large Stokes shift means that UVB and UVA are required to excite the RTP emitters, which would be harmful for organic and biological systems. Despite of their relatively short afterglow lifetimes, TADF afterglow emitters show relatively small Stokes shift (in some cases, TADF afterglow emitters can be sufficiently excited by visible lights) and the interference of excitation lights can be eliminated in the afterglow mode. Here, besides the spiroBF$_2$ RTP emitters, afterglow nanostructure fabrication can also be extended to TADF emitters. Recent studies show that TADF afterglow emitters can harvest triplet energy and improve afterglow efficiency.[44,45,82] TADF afterglow emulsion has been reported to show oxygen plus temperature sensing property in aqueous medium.[83] The current aqueous TADF afterglow systems are limited to spherical morphology, whereas other TADF afterglow nanostructures remain elusive.

© 2024 Wiley-VCH GmbH

23670932, 0, Downloaded from https://chemistry-europe.onlinelibrary.wiley.com/doi/10.1002/cptc.202400113 by Shanghai Institute Of Organic Chemistry, Wiley Online Library on [30/08/2024]. See the Terms and Conditions (https://onlinelibrary.wiley.com/terms-and-conditions) on Wiley Online Library for rules of use; OA articles are governed by the applicable Creative Commons License

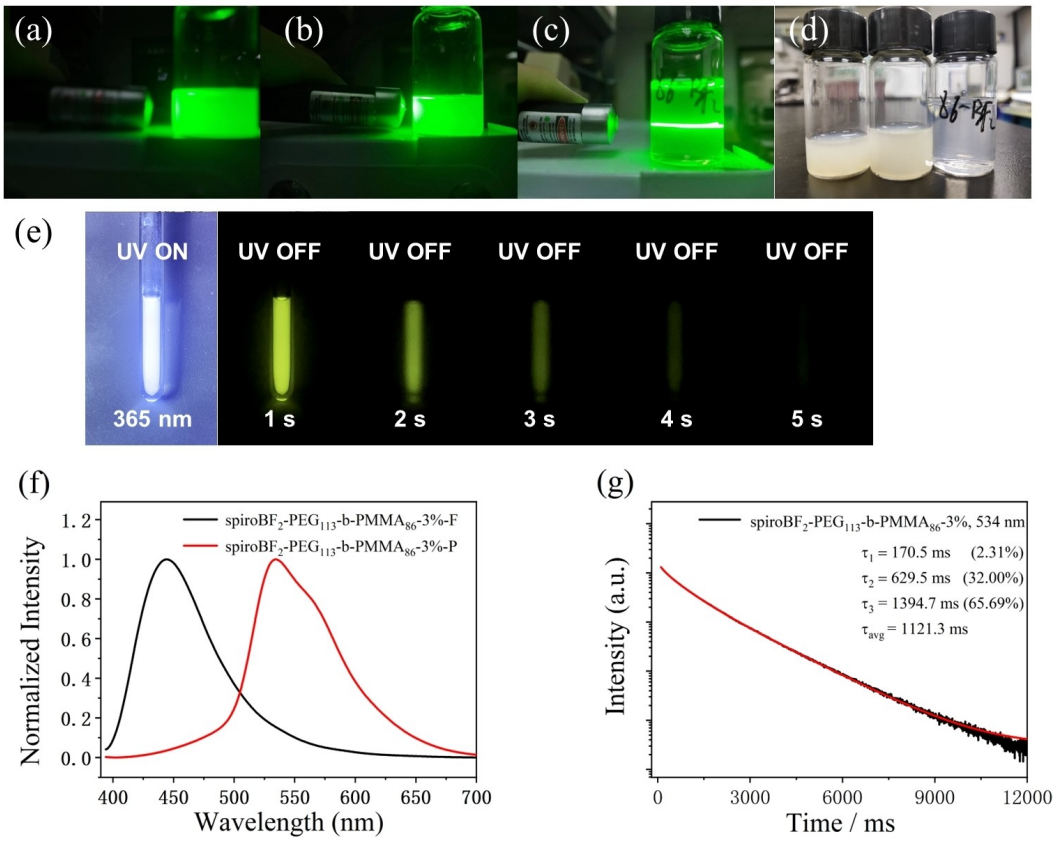

Figure 4. Photographs of (a) spiroBF$_2$-PEG$_{44}$-*b*-PMMA$_{136}$-3 %, (b) spiroBF$_2$-PEG$_{44}$-*b*-PMMA$_{203}$-3 % and(b) spiroBF$_2$-PEG$_{113}$-*b*-PMMA$_{86}$-3 % samples under the irradiation of a 530 nm laser pointer. (d) Photographs of spiroBF$_2$-PEG$_{44}$-*b*-PMMA$_{136}$-3 % sample (left), spiroBF$_2$-PEG$_{44}$-*b*-PMMA$_{203}$-3 % sample (middle) and spiroBF$_2$-PEG$_{113}$-*b*-PMMA$_{86}$-3 % sample (right). (e) Photographs of spiroBF$_2$-PEG$_{113}$-*b*-PMMA$_{86}$-3 % sample obtained under 365 nm UV and after switching-off the UV lamp at room temperature. (f) Steady-state emission and delayed emission (1 ms delay) spectra of spiroBF$_2$-PEG$_{113}$-*b*-PMMA$_{86}$-3 % sample excited by 374 nm at room temperature. (g) Excited state decay profile of spiroBF$_2$-PEG$_{113}$-*b*-PMMA$_{86}$-3 % sample excited by 374 nm and monitored at 534 nm at room temperature.

Here we select luminescent acridones, phOMeADT (Figure 2b), as TADF afterglow emitters. PEG$_{113}$-*b*-PMMA block copolymers with different PMMA lengths have been tested for the self-assembly. Dynamic light scattering (DLS) measurements show that the hydrodynamic diameters of phOMeADT-PEG$_{113}$-*b*-PMMA$_{55}$ and phOMeADT-PEG$_{113}$-*b*-PMMA$_{86}$ samples are 44 nm and 163 nm, respectively (Figure 5a and 5b). TEM observation exhibit that phOMeADT-PEG$_{113}$-*b*-PMMA$_{55}$ sample has mainly spherical morphology with average diameter of 38 nm (Figure 5c), which agrees with that by DLS measurement. In the case of phOMeADT-PEG$_{113}$-*b*-PMMA$_{86}$, worm-like morphology has been observed by TEM, exhibiting diameter of around 32 nm and average length of 156 nm (Figure 5d). The morphological transformation from spherical to worm-like nanostructures can be explained by the elongation of PMMA block and the increase hydrophobic/hydrophilic ratio. DLS measurement shows a hydrodynamic diameter of 163 nm with polydispersity index of 0.42, which is consistent with TEM observation. To our knowledge, it is the first time to observe a worm-like afterglow nanostructure in the field of organic RTP and afterglow materials. We also tried to prepare vesicle morphology by further increasing PMMA block length but failed; the long and hydrophobic PMMA chains in aqueous medium don't have sufficient flexibility to form polymeric vesicles with low curvature.

For the photophysical property, the delayed emission spectra (1 ms delay) of phOMeADT-PEG$_{113}$-*b*-PMMA$_{55}$-2 % sample at room temperature have been found to have similar band shape and similar emission maxima to the steady-state emission spectra (Figure 6a), with afterglow lifetimes of 0.2 to 0.3 s (Figure 6b). With reference to our previous studies on TADF afterglow systems and acridone-based TADF afterglow systems,[44,45,84,85] such observation suggests that phOMeADT-PEG$_{113}$-*b*-PMMA$_{55}$-2 % sample also shows TADF afterglow behavior in aqueous medium. Similar photophysical property is observed in phOMeADT-PEG$_{113}$-*b*-PMMA$_{86}$-2 % samples (Figure 6c and 6d). To gain an insight to this phOMeADT system, we perform photophysical measurements in its solution state and doped state. Its UV-vis spectrum exhibits a lower-energy band in the range of 370 nm to 450 nm and two higher-energy bands at 266 nm and 319 nm (Figure 7a). The 370–450 nm band can be assigned to S_0-to-S_1 transition that shows electronic transition within acridone backbone plus intramolecular charge transfer from anisole group to acridone backbone. Assisted by TD-DFT calculations (Figure 7c), the higher-energy bands at 266 nm and 319 nm can be assigned as S_0-to-S_4 and

© 2024 Wiley-VCH GmbH

23670932, 0, Downloaded from https://chemistry-europe.onlinelibrary.wiley.com/doi/10.1002/cptc.202400113 by Shanghai Institute Of Organic Chemistry, Wiley Online Library on [30/08/2024]. See the Terms and Conditions (https://onlinelibrary.wiley.com/terms-and-conditions) on Wiley Online Library for rules of use; OA articles are governed by the applicable Creative Commons License

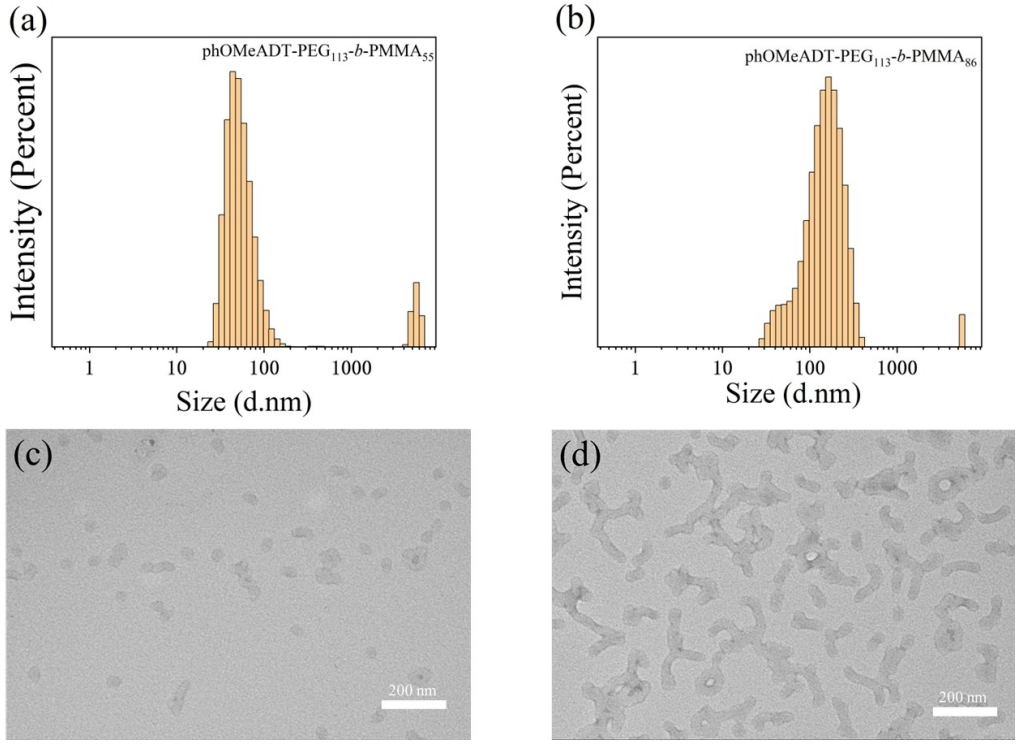

Figure 5. Hydrodynamic diameter distribution of (a) phOMeADT-PEG$_{113}$-*b*-PMMA$_{55}$ and (b) phOMeADT-PEG$_{113}$-*b*-PMMA$_{86}$ samples obtained by DLS study. TEM images of (c) phOMeADT-PEG$_{113}$-*b*-PMMA$_{55}$ and (d) phOMeADT-PEG$_{113}$-*b*-PMMA$_{86}$ samples.

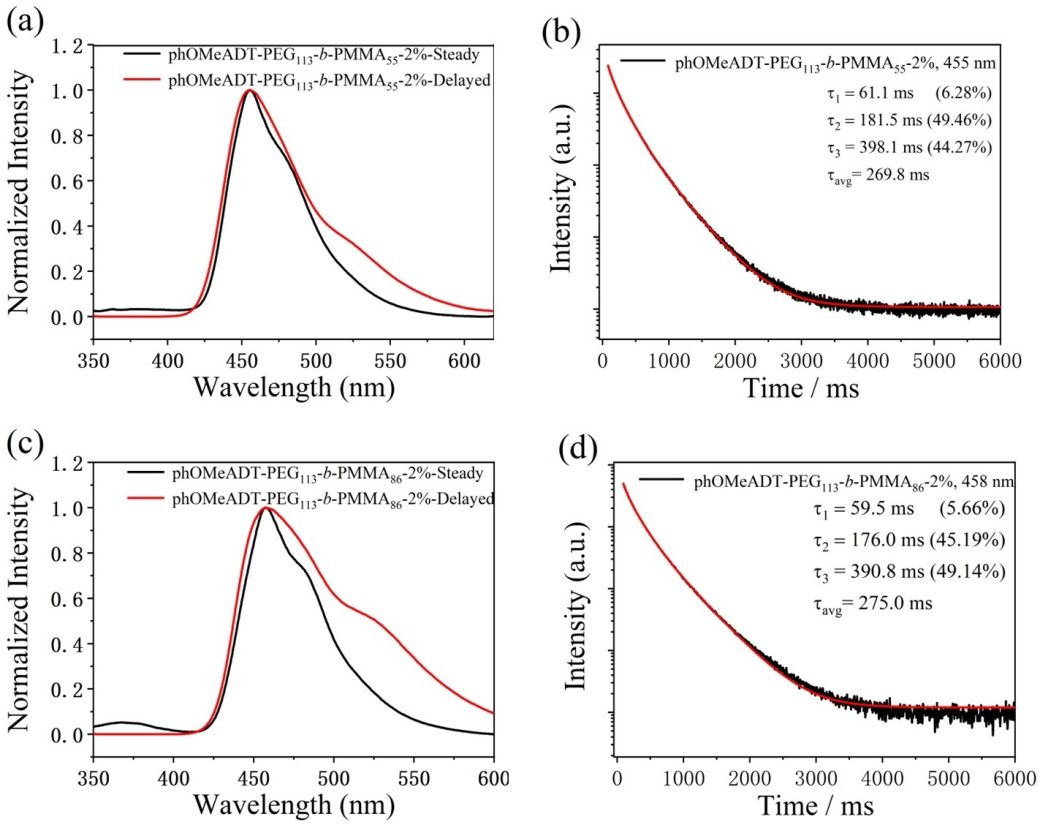

Figure 6. (a) Steady-state emission and delayed emission (1 ms delay) spectra of phOMeADT-PEG$_{113}$-*b*-PMMA$_{55}$-2% sample excited by 318 nm at room temperature. (b) Excited state decay profile (monitored at 455 nm) of phOMeADT-PEG$_{113}$-*b*-PMMA$_{55}$-2% sample excited by 318 nm at room temperature. (c) Steady-state emission and delayed emission (1 ms delay) spectra of phOMeADT-PEG$_{113}$-*b*-PMMA$_{86}$-2% sample excited by 323 nm at room temperature. (d) Excited state decay profile (monitored at 458 nm) of phOMeADT-PEG$_{113}$-*b*-PMMA$_{86}$-2% sample excited by 323 nm at room temperature.

© 2024 Wiley-VCH GmbH

23670932, 0, Downloaded from https://chemistry-europe.onlinelibrary.wiley.com/doi/10.1002/cptc.202400113 by Shanghai Institute Of Organic Chemistry, Wiley Online Library on [30/08/2024]. See the Terms and Conditions (https://onlinelibrary.wiley.com/terms-and-conditions) on Wiley Online Library for rules of use; OA articles are governed by the applicable Creative Commons License

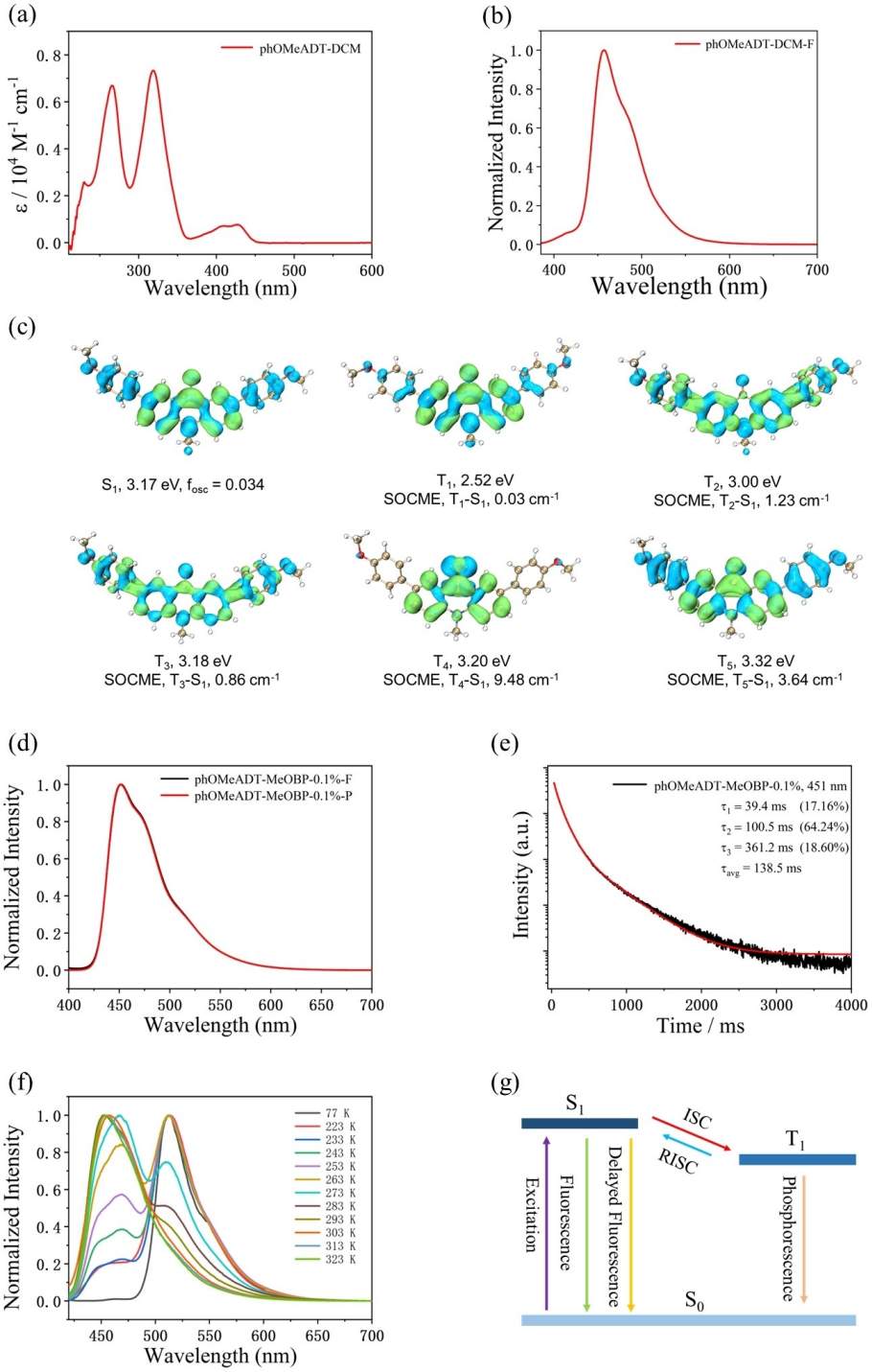

Figure 7. (a) UV-Vis spectra of phOMeADT in dichloromethane. (b) Room-temperature steady-state emission spectra of phOMeADT in dichloromethane. (c) TD-DFT calculation results of singlet excited states and triplet excited state of phOMeADT. (d) Steady-state emission and delayed emission (1 ms delay) spectra of phOMeADT-MeOBP-0.1 % sample excited by 374 nm at room temperature. (e) Excited state decay profile (monitored at 452 nm) of phOMeADT-MeOBP-0.1 % sample excited by 374 nm at room temperature. (f) Temperature-dependent delayed emission spectra (1 ms delay) of phOMeADT-MeOBP-0.1 % materials. (g) The proposed mechanism of the TADF-type organic afterglow in phOMeADT system at room temperature or higher temperature.

S_0-to-S_{10} transition, respectively (Figure S9). The steady-state emission spectrum of phOMeADT in dichloromethane shows fluorescence band from 420 to 550 nm with emission maxima at 457 nm (Figure 7b).

We also study the photophysical property of phOMeADT in doped state. Upon doping into 4-methoxybenzophenone (MeOBP), the resultant phOMeADT-MeOBP sample shows almost identical steady-state and delayed emission spectra at 452 nm (Figure 7d) with afterglow lifetime of 139 ms. At 77 K,

© 2024 Wiley-VCH GmbH

23670932, 0, Downloaded from https://chemistry-europe.onlinelibrary.wiley.com/doi/10.1002/cptc.202400113 by Shanghai Institute Of Organic Chemistry, Wiley Online Library on [30/08/2024]. See the Terms and Conditions (https://onlinelibrary.wiley.com/terms-and-conditions) on Wiley Online Library for rules of use; OA articles are governed by the applicable Creative Commons License

the delayed emission spectra (1 ms delay) exhibit the emergence of phosphorescence band at 513 nm in the lower-energy region. Temperature-dependent delayed spectra show the delayed fluorescence band at 455 nm increases with temperature and becomes dominant at room temperature or higher. Given the small doping concentration of 0.1 %, these observations are indicative of TADF-type afterglow of phOMeADT-MeOBP sample at room temperature (Figure 7g); at low doping concentration, delayed fluorescence by triplet-triplet annihilation should be insignificant.[86] The phOMeADT-MeOBP sample can be excited by visible light to emit room-temperature afterglow and MeOBP matrix has negligible absorption in visible region, so energy transfer from MeOBP to phOMeADT can be ruled out. Impurity-induced afterglow mechanism[87] can be rejected because of the high purity of phOMEADT as indicated by HPLC measurement (Figure S5). Our recent studies on narrowband multi-resonance TADF systems of acridones[84,85] also support the TADF afterglow mechanism in the present phOMeADT system (Figure 7g). It is known that the organic triplets are sensitive to oxygen and can be quenched by contacting oxygen. Here the MeOBP matrix exhibit a protective role for organic triplets due to their rigid crystalline structures, effectively insulating them from oxygen quenching. The singlet-triplet splitting energy (ΔE_{ST}) can be obtained from the fluorescence and phosphorescence maxima to be 0.31 eV. TD-DFT calculation shows that the excited state nature of S_1 and T_1 is similar to give a small spin-orbital coupling matrix element (SOCME) of 0.03 cm^{-1} in phOMeADT system (Figure 7c). Its T_2 and T_3 states have different symmetry from S_1 state, exhibiting SOCME values of 1.23 cm^{-1} and 0.86 cm^{-1}, respectively (Figure 7c). The T_2 and T_3 states can serve as a bridge for forward and reverse intersystem crossing. The rate constant of reverse intersystem crossing (k_{RISC}) at room temperature can be estimated from the TADF lifetime to be on the order of 10^0–10^1 s^{-1}. With reference to our previous studies,[44,45,84,85] the moderate k_{RISC} in the phOMeADT-MeOBP system agrees with the moderate ΔE_{ST} and rich intersystem crossing channels with moderate SOCME values. Given the nonradiative decay and oxygen quenching are sufficiently reduced in MeOBP matrix, the moderate k_{RISC} of 10^0–10^1 s^{-1} at room temperature would be enough to switch on TADF pathway in the phOMeADT system, because the phosphorescence decay rate in phOMeADT system would be on the order of 10^{-1}–10^0 s^{-1} (Figure 7e). With these studies on phOMeADT in solution state and doped state, we can understand the TADF afterglow property in phOMeADT-PEG-*b*-PMMA nanostructure system.

Conclusions

In conclusion, by merging our technology of two-component afterglow materials and block copolymer self-assembly, the present study successfully demonstrates the controlled fabrication of room-temperature organic afterglow nanostructures with intriguing photophysical property and well-defined morphology. The worm-like afterglow nanostructures have been firstly achieved in this study, which indicates the diverse opportunity in the miniaturization of organic afterglow materials for their promising applications. Further studies to realize other interesting morphologies via the techniques in polymer chemistry and physics are in progress.

Acknowledgements

We thank the financial supports from National Natural Science Foundation of China (22175194), the Strategic Priority Research Program of the Chinese Academy of Sciences (XDB0610000), Hundred Talents Program from Shanghai Institute of Organic Chemistry (Y121078), Pioneer Hundred Talents Program of Chinese Academy of Sciences (E320021), and Ningbo Natural Science Foundation (2023 J243).

Conflict of Interests

The authors declare no conflict of interest.

Data Availability Statement

The data that support the findings of this study are available from the corresponding author upon reasonable request.

Keywords: afterglow · block copolymers · nanostructures · phosphorescence · self-assembly

[1] V. W.-W. Yam, V. K.-M. Au, S. Y.-L. Leung, *Chem. Rev.* **2015**, *115*, 7589.
[2] W. Zhao, Z. He, B. Z. Tang, *Nat. Rev. Mater.* **2020**, *5*, 869.
[3] N. Gan, H. Shi, Z. An, W. Huang, *Adv. Funct. Mater.* **2018**, *28*, 1802657.
[4] X. Ma, J. Wang, H. Tian, *Acc. Chem. Res.* **2019**, *52*, 738.
[5] S. Hirata, *Adv. Opt. Mater.* **2017**, *5*, 1700116.
[6] A. Forni, E. Lucenti, C. Botta, E. Cariati, *J. Mater. Chem. C* **2018**, *6*, 4603.
[7] Kenry, C. Chen, B. Liu, *Nat. Commun.* **2019**, *10*, 2111.
[8] S. Guo, W. Dai, X. Chen, Y. Lei, J. Shi, B. Tong, Z. Cai, Y. Dong, *ACS Materials Lett.* **2021**, *3*, 379.
[9] X. Yan, H. Peng, Y. Xiang, J. Wang, L. Yu, Y. Tao, H. Li, W. Huang, R. Chen, *Small* **2022**, *18*, 2104073.
[10] H. Gao, X. Ma, *Aggregate* **2021**, *2*, e38.
[11] Q. Li, Z. Li, *Acc. Chem. Res.* **2020**, *53*, 962.
[12] H. Nie, Z. Wei, X. Ni, Y. Liu, *Chem. Rev.* **2022**, *122*, 9032.
[13] J. Guo, C. Yang, Y. Zhao, *Acc. Chem. Res.* **2022**, *55*, 1160.
[14] R. Kabe, C. Adachi, *Nature* **2017**, *550*, 384.
[15] O. Bolton, K. Lee, H.-J. Kim, K. Y. Lin, J. Kim, *Nat. Chem.* **2011**, *3*, 205.
[16] G. Zhang, G. M. Palmer, M. W. Dewhirst, C. L. Fraser, *Nat. Mater.* **2009**, *8*, 747.
[17] W. Z. Yuan, X. Y. Shen, H. Zhao, J. W. Y. Lam, L. Tang, P. Lu, C. Wang, Y. Liu, Z. Wang, Q. Zheng, J. Z. Sun, Y. Ma, B. Z. Tang, *J. Phys. Chem. C* **2010**, *114*, 6090.
[18] W. Zhao, Z. He, J. W. Y. Lam, Q. Peng, H. Ma, Z. Shuai, G. Bai, J. Hao, B. Z. Tang, *Chem* **2016**, *1*, 592.
[19] H. Ma, Q. Peng, Z. An, W. Huang, Z. Shuai, *J. Am. Chem. Soc.* **2019**, *141*, 1010.
[20] Z. Yang, C. Xu, W. Li, Z. Mao, X. Ge, Q. Huang, H. Deng, J. Zhao, F. L. Gu, Y. Zhang, Z. Chi, *Angew. Chem. Int. Ed.* **2020**, *59*, 17451.
[21] X.-F. Wang, H. Xiao, P.-Z. Chen, Q.-Z. Yang, B. Chen, C.-H. Tung, Y.-Z. Chen, L.-Z. Wu, *J. Am. Chem. Soc.* **2019**, *141*, 5045.
[22] H. Chen, X, Ma, S. Wu, H. Tian, *Angew. Chem. Int. Ed.* **2014**, *53*, 14149.
[23] B. Chen, W. Huang, H. Su, H. Miao, X. Zhang, G. Zhang, *Angew. Chem. Int. Ed.* **2020**, *59*, 10023–10026.

© 2024 Wiley-VCH GmbH

23670932, 0, Downloaded from https://chemistry-europe.onlinelibrary.wiley.com/doi/10.1002/cptc.202400113 by Shanghai Institute Of Organic Chemistry, Wiley Online Library on [30/08/2024]. See the Terms and Conditions (https://onlinelibrary.wiley.com/terms-and-conditions) on Wiley Online Library for rules of use; OA articles are governed by the applicable Creative Commons License

[24] X. K. Ma, W. Zhang, Z. Liu, H. Zhang, B. Zhang, Y. Liu, *Adv. Mater.* **2021**, *33*, 2007476.
[25] S. Hirata, K. Totani, J. Zhang, T. Yamashita, H. Kaji, S. R. Marder, T. Watanabe, C. Adachi, *Adv. Funct. Mater.* **2013**, *23*, 3386.
[26] H. Wu, W. Chi, Z. Chen, G. Liu, L. Gu, A. K. Bindra, G. Yang, X. Liu, Y. Zhao, *Adv. Funct. Mater.* **2019**, *29*, 1807243.
[27] I. Bhattacharjee, S. Hirata, *Adv. Mater.* **2020**, *32*, 2001348.
[28] Z. Yang, Z. Mao, X. Zhang, D. Ou, Y. Mu, Y. Zhang, C. Zhao, S. Liu, Z. Chi, J. Xu, Y.-C. Wu, P.-Y. Lu, A. Lien, M. R. Bryce, *Angew. Chem. Int. Ed.* **2016**, *55*, 2181.
[29] Z. An, C. Zheng, Y. Tao, R. Chen, H. Shi, T. Chen, Z. Wang, H. Li, R. Deng, X. Liu, W. Huang, *Nat. Mater.* **2015**, *14*, 685.
[30] Y. Wang, J. Yang, M. Fang, Y. Yu, B. Zou, L. Wang, Y. Tian, J. Cheng, B. Z. Tang, Z. Li, *Matter* **2020**, *3*, 449.
[31] J. Mei, N. L. C. Leung, R. T. K. Kwok, J. W. Y. Lam, B. Z. Tang, *Chem. Rev.* **2015**, *115*, 11718.
[32] T. Zhang, X. Ma, H. Wu, L. Zhu, Y. Zhao, H. Tian, *Angew. Chem. Int. Ed.* **2020**, *59*, 11206.
[33] J. Wang, Z. Huang, X. Ma, H. Tian, *Angew. Chem. Int. Ed.* **2020**, *59*, 9928.
[34] Z.-Y. Zhang, Y. Chen, Y. Liu, *Angew. Chem. Int. Ed.* **2019**, *58*, 6028.
[35] K. Jinnai, R. Kabe, Z. Lin, C. Adachi, *Nat. Mater.* **2022**, *21*, 338.
[36] Z. Lin, R. Kabe, K. Wang, C. Adachi, *Nat. Commun.* **2020**, *11*, 191.
[37] P. Alam, T. S. Cheung, N. L. C. Leung, J. Zhang, J. Guo, L. Du, R. T. K. Kwok, J. W. Y. Lam, Z. Zeng, D. L. Phillips, H. H. Y. Sung, I. D. Williams, B. Z. Tang, *J. Am. Chem. Soc.* **2022**, *144*, 3050.
[38] X. Liang, Y.-X. Zheng, J.-L. Zuo, *Angew. Chem. Int. Ed.* **2021**, *60*, 16984.
[39] X. Deng, J. Huang, G. Wang, J. Li, X. Li, C. Lei, K. Zhang, *Chem. Commun.* **2022**, *58*, 8137.
[40] Z. Mo, G. Wang, J. Li, Q. Yan, K. Zhang, *J. Phys. Chem. Lett.* **2023**, *14*, 11142.
[41] Y. Lei, W. Dai, J. Guan, S. Guo, F. Ren, Y. Zhou, J. Shi, B. Tong, Z. Cai, J. Zheng, Y. Dong, *Angew. Chem. Int. Ed.* **2020**, *59*, 16054.
[42] Y. Sun, J. Liu, J. Li, X. Li, X. Wang, G. Wang, K. Zhang, *Adv. Opt. Mater.* **2022**, *10*, 2101909.
[43] P. D. Ronald, H. K. Evan, *J. Polym. Biopolym. Phys. Chem.* **2023**, *11*, 1.
[44] X. Wang, Y. Sun, G. Wang, J. Li, X. Li, K. Zhang, *Angew. Chem. Int. Ed.* **2021**, *60*, 17138.
[45] Y. Pan, J. Li, X. Wang, Y. Sun, J. Li, B. Wang, K. Zhang, *Adv. Funct. Mater.* **2021**, *32*, 2110207.
[46] S. Xu, W. Wang, H. Li, J. Zhang, R. Chen, S. Wang, C. Zheng, G. Xing, C. Song, W. Huang, *Nat. Commun.* **2020**, *11*, 4802.
[47] J.-X. Wang, H. Zhang, L.-Y. Niu, X. Zhu, Y.-F. Kang, R. Boulatov, Q.-Z. Yang, *CCS Chem.* **2020**, *2*, 1391.
[48] S. Kuila, S. J. George, *Angew. Chem. Int. Ed.* **2020**, *59*, 9393.
[49] Q. Dang, Y. Jiang, J. Wang, J. Wang, Q. Zhang, M. Zhang, S. Luo, Y. Xie, K. Pu, Q. Li, Z. Li, *Adv. Mater.* **2020**, *32*, 2006752.
[50] F. Lin, H. Wang, Y. Cao, R. Yu, G. Liang, H. Huang, Y. Mu, Z. Yang, Z. Chi, *Adv. Mater.* **2022**, *34*, 2108333.
[51] X. Zhen, Y. Tao, Z. An, P. Chen, C. Xu, R. Chen, W. Huang, K. Pu, *Adv. Mater.* **2017**, *29*, 1606665.
[52] M. Gmelch, T. Achenbach, A. Tomkeviciene, S. Reineke, *Adv. Sci.* **2021**, *8*, 2102104.
[53] X. Yao, J. Wang, D. Jiao, Z. Huang, O. Mhirsi, F. Lossada, L. Chen, B. Haehnle, A. J. C. Kuehne, X. Ma, H. Tian, A. Walther, *Adv. Mater.* **2021**, *33*, 2005973.
[54] Y. Su, Y. Zhang, Z. Wang, W. Gao, P. Jia, D. Zhang, C. Yang, Y. Li, Y. Zhao, *Angew. Chem. Int. Ed.* **2020**, *59*, 9967.
[55] F. Xiao, H. Gao, Y. Lei, W. Dai, M. Liu, X. Zheng, Z. Cai, X. Huang, H. Wu, D. Ding, *Nat. Commun.* **2022**, *13*, 186.
[56] C. Qian, Z. Ma, X. Fu, X. Zhang, Z. Li, H. Jin, M. Chen, H. Jiang, X. Jia, Z. Ma, *Adv. Mater.* **2022**, *34*, 2200544.
[57] J. Han, W. Feng, D. Y. Muleta, C. N. Bridgmohan, Y. Dang, G. Xie, H. Zhang, X. Zhou, W. Li, L. Wang, D. Liu, Y. Dang, T. Wang, W. Hu, *Adv. Funct. Mater.* **2019**, *29*, 1902503.
[58] Y. Yu, M. S. Kwon, J. Jung, Y. Zeng, M. Kim, K. Chung, J. Gierschner, J. H. Youk, S. M. Borisov, J. Kim, *Angew. Chem. Int. Ed.* **2017**, *56*, 16207.
[59] J. Huang, X. Deng, J. Li, G. Wang, X. Li, H. Yao, C. Lei, K. Zhang, *Chem. Eng. J.* **2023**, *474*, 145809.
[60] N. Bertrand, J. Wu, X. Xu, N. Kamaly, O. C. Farokhzad, *Cancer Nanotechnol.* **2014**, *66*, 2.
[61] G. Gaucher, M.-H. Dufresne, V. P. Sant, N. Kang, D. Maysinger, J.-C. Leroux, *J. Controlled Release* **2005**, *109*, 169.
[62] J. F. Kukowska-Latallo, K. A. Candido, Z. Y. Cao, S. S. Nigavekar, I. J. Majoros, T. P. Thomas, L. P. Balogh, M. K. Khan, J. R. Baker, *Cancer Res.* **2005**, *65*, 5317.
[63] C. Khemtong, C. W. Kessinger, J. M. Gao, *Chem. Commun.* **2009**, 3497.
[64] Y. Geng, P. Dalhaimer, S. Cai, R. Tsai, M. Tewari, T. Minko, D. E. Discher, *Nat. Nanotechnol.* **2007**, *2*, 249.
[65] F. Tantakitti, J. Boekhoven, X. Wang, R. V. Kazantsev, T. Yu, J. Li, E. Zhuang, R. Zandi, J. H. Ortony, C. J. Newcomb, L. C. Palmer, G. S. Shekhawat, M. O. de la Cruz, G. C. Schatz, S. I. Stupp, *Nat. Mater.* **2016**, *15*, 469.
[66] X. Q. Liu, K. Zhang, J. F. Gao, Y. Z. Chen, C. H. Tung, L. Z. Wu, *Angew. Chem. Int. Ed.* **2020**, *59*, 23456.
[67] J. Liu, Y. Sun, G. Wang, X. Chen, J. Li, X. Wang, Y. Zou, B. Wang, K. Zhang, *Adv. Opt. Mater.* **2022**, *10*, 2201502.
[68] X. Zhai, Y. Zeng, X. Deng, Q. Lou, A. Cao, L. Ji, Q. Yan, B. Wang, K Zhang, *Chem. Commun.* **2023**, *59*, 10500.
[69] L. F. Zhang, A. Eisenberg, *Science* **1995** *268*, 1728.
[70] S. Jain, F. S. Bates, *Science* **2003**, *300*, 460.
[71] Z. B. Li, E. Kesselman, Y. Talmon, M. A. Hillmyer, T. P. Lodge, *Science* **2004**, *306*, 98.
[72] J. Massey, K. N. Power, I. Manners, M. A. Winnik, *J. Am. Chem. Soc.* **1998**, *120*, 9533.
[73] H. G. Cui, Z. Y. Chen, S. Zhong, K. L. Wooley, D. J. Pochan, *Science* **2007**, *317*, 647.
[74] I. Dimitrov, B. Trzebicka, A. H. E. Müller, A. Dworak, C. B. Tsvetanov, *Prog. Polym. Sci.* **2007**, *32*, 1275.
[75] D. Y. Chen, M. Jiang, *Acc. Chem. Res.* **2005**, *38*, 494.
[76] M. Guo, M. Jiang, *Soft Matter* **2009**, *5*, 495.
[77] M. Huang, U. Schilde, M. Kumke, M. Antonietti, H. Cölfen, *J. Am. Chem. Soc.* **2010**, *132*, 3700.
[78] A. F. Thünemann, S. Kubowicz, C. Burger, M. D. Watson, N. Tchebotareva, K. Müllen, *J. Am. Chem. Soc.* **2003**, *125*, 352.
[79] K. Zhang, M. C.-L. Yeung, S. Y.-L. Leung, V. W.-W. Yam, *J. Am. Chem. Soc.* **2018**, *140*, 9594.
[80] K. Zhang, M. C.-L. Yeung, S. Y.-L. Leung, V. W.-W. Yam, *Proc. Natl. Acad. Sci. USA* **2017**, *114*, 11844.
[81] K. Zhang, M. C.-L. Yeung, S. Y.-L. Leung, V. W.-W. Yam, *Chem* **2017**, *2*, 825.
[82] H. Uoyama, K. Goushi, K. Shizu, H. Nomura, C. Adachi, *Nature* **2012**, *492*, 234.
[83] H. Yao, Y. Zhang, G. Wang, J. Li, J. Huang, X. Wang, Z. Zhang, L. Chen, Z. Pan, K Zhang, *ACS Appl. Nano Mater.* **2023**, *6*, 15138.
[84] G. Wang, S. Ding, J. Li, Z Ye, W. Xia, X. Chen, K. Zhang, *Chem. Commun.* **2023**, *59*, 12302.
[85] G. Wang, S. Ding, J. Li, X. Li, W. Xia, X. Chen, H. Yao, Z. Ye, K. Zhang, *Chem. Mater.* **2024**, *36*, 3000.
[86] Z. Lin, R. Kabe, K. Wang, C. Adachi, *Nat. Commun.* **2020**, *11*, 191.
[87] C. Chen, Z. Chi, K. C. Chong, A. S. Batsanov, Z. Yang, Z. Mao, Z. Yang, B. Liu, *Nat. Mater.* **2021**, *20*, 175.

Manuscript received: March 30, 2024
Revised manuscript received: May 11, 2024
Accepted manuscript online: May 31, 2024
Version of record online: ■■, ■■

© 2024 Wiley-VCH GmbH

23670932, 0, Downloaded from https://chemistry-europe.onlinelibrary.wiley.com/doi/10.1002/cptc.202400113 by Shanghai Institute Of Organic Chemistry, Wiley Online Library on [30/08/2024]. See the Terms and Conditions (https://onlinelibrary.wiley.com/terms-and-conditions) on Wiley Online Library for rules of use; OA articles are governed by the applicable Creative Commons License

RESEARCH ARTICLE

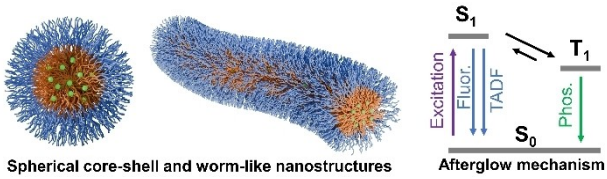

Y. Zhang, X. Chen, T. Wang, Z. Mo, G. Wang, H. Li, K. Zhang**

Miniaturization of organic afterglow materials has shown promising applications, whereas current technologies lack the capability of facile control on the morphology and dimension of the miniaturized afterglow materials. This study presents controlled fabrication of spherical core-shell and worm-like organic afterglow nanostructures via block copolymer self-assembly and dopant-matrix strategy at room temperature.

23670932, 0, Downloaded from https://chemistry-europe.onlinelibrary.wiley.com/doi/10.1002/cptc.202400113 by Shanghai Institute Of Organic Chemistry, Wiley Online Library on [30/08/2024]. See the Terms and Conditions (https://onlinelibrary.wiley.com/terms-and-conditions) on Wiley Online Library for rules of use; OA articles are governed by the applicable Creative Commons License